Research Article | Vol. 25, No. 21 | 16 Oct 2017 | OPTICS EXPRESS 25741
Optics EXPRESS

Subcutaneous veins depth measurement using diffuse reflectance images

C. M. GOH,[1,2] R. SUBRAMANIAM,[3] N. M. SAAD,[1] S. A. ALI,[1] AND F. MERIAUDEAU[1,2,*]

[1]*Center for Intelligent Signal & Imaging Research (CISIR), Department of Electrical and Electronic Engineering, Universiti Teknologi PETRONAS, 32610, Seri Iskandar, Perak, Malaysia*
[2]*LE2I FRE 2305, CNRS, ENSAM, Univ. Bourgogne Franche-Comte, France*
[3]*Department of Radiology, Unikl Royal College of Medicine, 30450, Ipoh, Perak, Malaysia*
[*]*fabrice.meriaudeau@utp.edu.my*

Abstract: Intravenous (IV) procedures are often difficult due to the poor visualization of subcutaneous veins. Because existing vein locators lack the ability to assess depth, and also because mis-punctures and poor vascular access remain problematic, we propose an imaging system that employs diffuse reflectance images at three isosbestic wavelengths to measure both the depth and thickness of subcutaneous veins. This paper describes the proposed system as well as proof-of-principle experimental demonstrations. We initially introduce the working principle and structure of the system. All measurements were based on the Monte Carlo (MC) method and accomplished by referring an optical density (OD) ratio to a multi-layer diffuse reflectance model. Results were all validated by comparative ultrasound measurements. Experimental trials included 11 volunteers who were subjected to both ultrasound measurements and the proposed optical process to validate the system's applicability. However, the unreliability of the "thickness" measurement of the vein may be due to the fact that the veins have collapsible walls – so excess pressure by the transducer will give a false thickness.

OCIS codes: (110.0110) Imaging systems; (100.0100) Image processing; (120.0120) Instrumentation, measurement, and metrology.

References and links

1. L. Hadaway, "Development of an infusion alliance," J. Infus. Nurs. **33**(5), 278–290 (2010).
2. O. O. Nafiu, C. Burke, A. Cowan, N. Tutuo, S. Maclean, and K. K. Tremper, "Comparing peripheral venous access between obese and normal weight children," Paediatr. Anaesth. **20**(2), 172–176 (2010).
3. AccuVein AV300 Vein viewing system,"catalog.kpnfs.com/equipcat/cutsheets2/VEFI200-C.pdf.,"
4. Vein locator BS2000 +, " http://img.tjskl.org.cn/nimg/41/6a/8b7a318853ec0c2f678efa44408b-98x98–1/vein_viewing_medical_light_doctor_costume_accessories_use_safe_light_source_no_laser.jpg.,".
5. Veinlite, "http://www.veinlite.com/purchasing-agents/#.U7vQqfldWmE.
6. N. J. Cuper, J. H. G. Klaessens, J. E. N. Jaspers, R. de Roode, H. J. Noordmans, J. C. de Graaff, and R. M. Verdaasdonk, "The use of near-infrared light for safe and effective visualization of subsurface blood vessels to facilitate blood withdrawal in children," Med. Eng. Phys. **35**(4), 433–440 (2013).
7. Luminetx Vein Viwer, http://www.ohgizmo.com/2006/11/15/luminetx-veinviewer/#!baJYx2.
8. Veinsite hands-free system, "http://www.vision-systems.com,".
9. A. Shahzad, M. N. Saad, N. Walter, A. S. Malik, and F. Meriaudeau, "Hyperspectral Venous Image Quality Assessment for Optimum Illumination Range Selection Based on Skin Tone Characteristics," Biomed. Eng. Online **13**(1), 109 (2014).
10. V. C. Paquit, K. W. Tobin, J. R. Price, and F. Mèriaudeau, "3D and Multispectral Imaging for Subcutaneous Veins Detection," Opt. Express **17**(14), 11360–11365 (2009).
11. V. Paquit, J. R. Price, R. Seulin, F. Meriaudeau, R. H. Farahi, K. W. Tobin, and T. L. Ferrell, "Near-infrared imaging and structured light ranging for automatic catheter insertion," Med. Imaging, Int. Soc. Opt. Photonics **6141**, 61411T (2008).
12. D. Ai, J. Yang, J. Fan, Y. Zhao, X. Song, J. Shen, L. Shao, and Y. Wang, "Augmented reality based real-time subcutaneous vein imaging system," Biomed. Opt. Express **7**(7), 2565–2585 (2016).
13. M. Poetke and H. P. Berlien, "Laser treatment in hemangiomas and vascular malformations," Med. Laser Appl. **20**(2), 95–102 (2005).

#295885 https://doi.org/10.1364/OE.25.025741
Journal © 2017 Received 15 May 2017; revised 3 Aug 2017; accepted 3 Aug 2017; published 10 Oct 2017

Optics EXPRESS

14. C. T. W. Lahaye and M. J. C. van Gemert, "Optimal laser parameters for port wine stain therapy: a theoretical approach," Phys. Med. Biol. **30**(6), 573–587 (1985).
15. M. J. C. van Gemert, A. J. Welch, and A. P. Amin, "Is there an optimal laser treatment for port wine stains?" Lasers Surg. Med. **6**(1), 76–83 (1986).
16. J. W. Tunnell, L. V. Wang, and B. Anvari, "Optimum pulse duration and radiant exposure for vascular laser therapy of dark port-wine skin: a theoretical study," Appl. Opt. **42**(7), 1367–1378 (2003).
17. A. A. Esenaliev, A. A. Karabutov, and A. A. Oraevsky, "Sensitivity of laser opto-acoustic imaging in detection of small deeply embedded tumors," IEEE J. Sel. Top. Quantum Electron. **5**(4), 981–988 (1999).
18. J. S. Nelson, T. E. Milner, B. S. Tanenbaum, D. M. Goodman, and M. J. C. Van Gemert, "Infra-red tomography of port-wine-stain blood vessels in human skin," Lasers Med. Sci. **11**(3), 199–204 (1996).
19. B. P. Payne, V. Venugopalan, B. B. Mikić, and N. S. Nishioka, "Optoacoustic tomography using time-resolved interferometric detection of surface displacement," J. Biomed. Opt. **8**(2), 273–280 (2003).
20. S. L. Jacques, I. S. Saidi, and F. K. Tittel, "Average depth of blood vessels in skin and lesions deduced by optical fiber spectroscopy," Int. Soc. Opt. Photonics **2128**, 231–237 (1994).
21. I. Nishidate, T. Maeda, Y. Aizu, and K. Niizeki, "Visualizing depth and thickness of a local blood region in skin tissue using diffuse reflectance images," J. Biomed. Opt. **12**(5), 054006 (2007).
22. I. Nishidate, Y. Aizu, and H. Mishina, "Depth visualization of a local blood region in skin tissue by use of diffuse reflectance images," Opt. Lett. **30**(16), 2128–2130 (2005).
23. T. Iwai and G. Kimura, "Imaging of an absorbing object embedded in a dense scattering medium by diffusing light topography," Opt. Rev. **7**(5), 436–441 (2000).
24. A. Chen, K. Nikitczuk, J. Nikitczuk, T. Maguire, and M. Yarmush, "Portable robot for autonomous venipuncture using 3D near infrared image guidance," Technology (Singap World Sci) **1**(1), 72–87 (2013).
25. C. Zhu and Q. Liu, "Review of Monte Carlo modeling of light transport in tissues," J. Biomed. Opt. **18**(5), 050902 (2013).
26. S. T. Flock, M. S. Patterson, B. C. Wilson, and D. R. Wyman, "Monte Carlo modeling of light propagation in highly scattering tissue - I: Model predictions and comparison with diffusion theory," IEEE Trans. Biomed. Eng. **36**(12), 1162–1168 (1989).
27. L. Wang, S. L. Jacques, and L. Zheng, "MCML - Monte Carlo modeling of light transport in multi-layered tissues," Comput. Methods Programs Biomed. **47**(2), 131–146 (1995).
28. S. L. Wang, "Monte Carlo Modeling of light transport in multilayer tissue.pdf,".
29. S. A.-E. Erik Alerstam, "Monte Carlo Simulations of Light Transport in Tissue," 1–12 (2008).
30. S. L. Jacques, "Skin Optics," .
31. I. Nishidate, Y. Aizu, and H. Mishina, "Estimation of absorbing components in a local layer embedded in the turbid media on the basis of visible to near-infrared (VIS-NIR) reflectance spectra," Opt. Rev. **10**(5), 427–435 (2003).
32. I. Nishidate, Y. Aizu, and H. Mishina, "Estimation of melanin and hemoglobin in skin tissue using multiple regression analysis aided by Monte Carlo simulation," J. Biomed. Opt. **9**(4), 700–710 (2004).
33. A. F. Frangi, W. J. Niessen, K. L. Vincken, and M. A. Viergever, "Multiscale vessel enhancement filtering," Medial Image Comput. Comput. Invervention - MICCAI'98. Lect. Notes Comput. Sci. **1496**(1496), 130–137 (1998).
34. V. Paquit, J. R. Price, F. Mériaudeau, K. W. Tobin, Jr., and T. L. Ferrell, "Combining near-infrared illuminants to optimize venous imaging," Proc. SPIE **6509**, 65090H (2007).
35. G. Zonios, J. Bykowski, and N. Kollias, "Skin melanin, hemoglobin, and light scattering properties can be quantitatively assessed in vivo using diffuse reflectance spectroscopy," J. Invest. Dermatol. **117**(6), 1452–1457 (2001).
36. J. Whitman, M. P. Fronheiser, and S. W. Smith, "3-D ultrasound guidance of surgical robotics using catheter transducers: Feasibility study," IEEE Trans. Ultrason. Ferroelectr. Freq. Control **55**, 993–996 (2008).

1. Introduction

Peripheral Difficult Venous Access (PDVA) is common and occurs daily in clinical conditions due to poorly visualized subcutaneous veins that are difficult to view in the visible light spectrum, especially for infants, hairy patients, those with dark skin color and obese individuals. Repeated puncture attempts also damage veins and cause discomfort, in addition to incurring extra labor and material costs. An American study reported sales of 300 million peripheral intravenous catheters (PIVCs) [1] and first time IV success rates of 74–88% and 46–76% [2] for the general population and children, respectively. Consequently, various near-infrared imaging vein locator devices have been developed. These include the AccuVein AV300 Vein viewing system [3]; Vein locator BS2000 + [4]; Veinlite [5]; VascuLuminator [6]; Luminetx Vein Viewer [7] and the Veinsite hands-free system [8]. All were developed to improve vein localization for IV access. They have demonstrated improved accuracy for venous access procedures but provide no data regarding venous depth or size. As such, they

Optics EXPRESS

do not assist deep needle insertions, which means that IV access, in many cases, remains dependent on clinical skills and still allows higher mis-puncture rates and costs.

Apart from commercial devices, researchers have proposed enhancement approaches that include vein detection [9], optimized illumination [9], combining 3D forearm data with vein visualization [10-11], and augmented reality visualization procedures to improve IV injection success rates [12]. The latest augmented reality system [12] has demonstrated performance efficiency by projecting augmented planar venous structures to the skin surface of the forearm to assist visualization. Another system [11] constructs a 3-D map of subcutaneous veins that guides catheter orientation for IV procedures. For both systems, authors have reported that depth information can be produced via 3D imaging reconstruction but the technique has not yet been validated with real data.

Other than assisting IV access, a depth profile is useful for procedures such as the laser treatment of port wine stains, etc [13–16], as well as for diagnostic processes such as breast tumor detection [17]. Depth data optimizes radiant exposure to light pulse duration in the treatment of port wine stains. Various techniques are in use to determine venous depth profiles, including the fast infrared focal plane array camera [18] and optoacoustic imaging [19]. Such techniques have demonstrated efficient in-vivo subsurface imaging but require a pulsed laser source that is both expensive and problematic. From the state of the art, diffuse reflectance imaging could be used as an alternative approach to profile the venous depth [20–23]. Here, depth measurement is achieved by employing an optical density (OD) ratio between two diffuse reflectance images.

Compared to pulsed laser sourcing, NIR transillumination is simple and costs less. Jacques et al. [20] developed the technique using an OD ratio between two isosbestic wavelengths (420 and 585 nm) to estimate subcutaneous venous depth. However, their model did not account for melanosomal effects. Hence, the OD ratio varied due to differential absorption levels caused by melanosomes in the stratum corneum. Nishidate et al. [21-22] have since improved the model by including the concentration of melanin as a variable. They proposed a new OD ratio (OD_{420}/OD_{800}) to measure subcutaneous venous thickness, claiming that *depth* and *thickness* could be measured by using a comparative tissue-like agar gel phantom (as reference). They produced accuracy rates of 94 and 78%, respectively, and consequently reported in-vivo accuracy rates of 70 and 81%, respectively, on experimental application. Several other techniques have been reported [23-24], also based on diffuse reflectance. These techniques demonstrate different concepts to infer depth via absorptive media. However, hemoglobin's oxygenation plus variations in melenasomal concentration have produced unreliable depth measurements [22].

The concept of measuring the veins depth and thickness using OD ratio deserved to be applied in the real-world due to its low cost, non-invasive properties and from the fact that it is a non-skin contact measurement technique. This paper therefore proposes an enhanced solution for the problem of estimating venous depth with the design of a new system that was experimentally confirmed using results from 66 measurement points taken from 11 subjects and validated with ultrasound imaging. Test subjects with four types of skin tone as well as different Body Mass Indexes (BMI) were used to confirm the proposed system's applicability. Moreover, in the future, human dependent catheterization could be replaced by a fully automated robotic system [24]. Such a system requires accurate depth and thickness data to optimize needle insertion and thus gain IV access. This research therefore presents an imaging system that visualizes and measures the depth and thickness of subcutaneous veins based on the Monte Carlo (MC) method. We employed the MC method to generate diffuse reflectance as the gold standard [25] for modeling light transport in turbid media. It also offers flexible responses with desired accuracy [26] as a solution to the problem posed by the radioactive transport equation (RTE) in turbid media containing complex structures. Our proposed system relies on two pillars: (1) OD ratios obtained from a calibrated multispectral system; and (2) a model of steady-state light transport in multi-layered tissues (MCML) [27],

Optics EXPRESS

which is used to infer venous depth and thickness from acquired diffuse reflectance images. Images at three isosbestic wavelengths for hemoglobin (420, 585 and 800 nm) were employed to obtain OD ratio images in a manner similar to that proposed by Nishidate et al. [21]. OD ratios are then referred to the diffuse reflectance model to infer subcutaneous venous depth and thickness. To clarify our position, Fig. 1 illustrates subcutaneous venous and its depth and thickness in a bi-layered skin model. Depth is defined as the distance from the skin's surface to the upper surface of a vein; thickness is the measured distance from the anterior to the posterior wall of a vein. NB: this study assumes that melanosomes and hemoglobin are homogenously distributed in epidermal and dermis layer respectively [21]. The vein is considered as planar and the simulations were done using the compiled code for light propagation modeling [28,29]. We didn't try to implement a more accurate model for the vein because a good accuracy has been achieved in the work of Nishidate et. al. [21] as compared to physical phantom made of agar gel solutions.

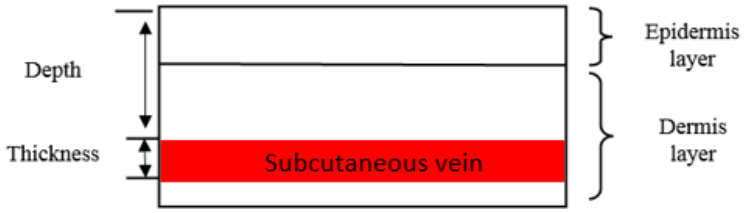

Fig. 1. Multilayered skin tissue model.

This paper has five sections. Section 1 presents the study's background and objectives; Section 2 describes relevant theories; Section 3 explains the devices used to build the proposed system and our experimental procedures; Section 4 presents experimental outcomes, data collection, and analysis; Section 5 concludes this work with a discussion of findings and proposes future research.

2. State of the art

2.1 Multi-layer diffuse reflectance model

The proposed system determines venous depth by using the ratio of OD_{420} to OD_{585}, designated as R1; and venous thickness by using the ratio of OD_{420} to OD_{800}, designated as R2. Theoretically, depth is determined as a function of R1 and is independent of the thickness, whereas thickness is determined as a function of R2 at a specific depth. To specify the relation between R1 and R2 with respect to depth and thickness, the MCML program [27] was used to generate diffuse reflectance models at different depths and thicknesses for the bi-layered skin model. This simulated data then served to infer depth and thickness, respectively, while also comparing estimates to reflectance measurements taken by the proposed optical system. Figure 2(a)-2(b) show the evolution of R1 and R2 (depth and thickness), respectively. In both cases diffuse reflectance data were simulated with concentration volumes for melanosomes (C_m) and blood (C_b) at 4.0 and 0.2%, respectively; depth and thickness values were set at 1 mm. The graphs show that R1 and R2 varied according to depth (d) and thickness (t), respectively. R1 increases as vein depth increases, whereas R2 decreases with vein thickness. In both cases, OD at 420 nm remained constant; hence, it was used as a constant parameter (numerator) to compute both R1 and R2 ratios. Meanwhile, OD at 585 nm varied as vein depth increased but remained constant as veins thickened, and was thus employed as a denominator to determine depth. On the other hand, OD at 800 nm varied according to depth and thickness, and also showed greater penetration; therefore, it was used as denominator to infer vein thickness. These factors were proposed by Nishidate et al. [21], who used R1 to measure depth independent of R2, which was used to measure thickness for a known depth ranging between 0.2 and 2.0 mm [21].

Optics EXPRESS

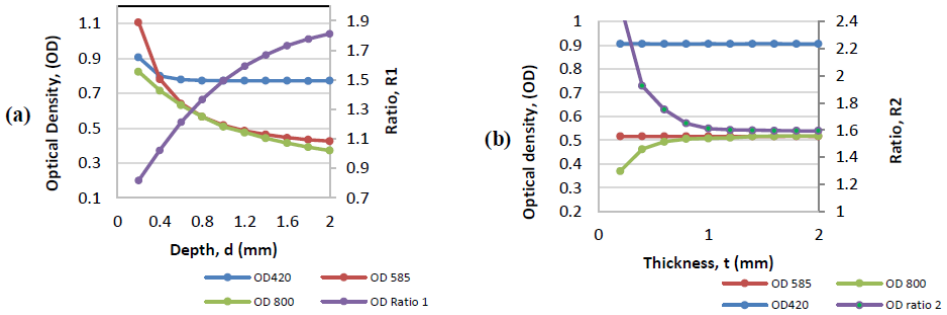

Fig. 2. (a) Dependent on OD ratio 1 (R1) for depth; (b) Dependent on OD ratio 2 (R2) for thickness; both values derived from MCML simulations.

As discussed above, models of diffuse reflectance for multi-layered skin need to be independently created to serve as references for R1 and R2 values that infer depth and thickness estimates for subcutaneous veins. Light distribution is thus simulated at depths and thicknesses ranging between 0.2 to 2 mm at intervals of 0.2 mm. The range of 0.2-2.0mm is set based on the shallowest penetration to the deepest penetration of light into the skin layer at a certain wavelength (i.e. 420nm, 585nm, and 800nm) and also the most superficial position of the vein is located. The light of wavelength 420nm penetrates the shallowest depth of the skin at about 0.1mm while the light of wavelength 800nm penetrates to a deepest level of 5mm. In order to compare our result with the previous study [21], we use the same limit; which assumed that the depth and thickness of subcutaneous veins is at the range of 0.2-2mm (interval of 0.2mm). Other than that, this system is limited to measure the depth of superficial and subcutaneous veins but not the deep veins. The absorption coefficient for the epidermis ($\mu_{a,epi}$) depends on the concentration of melanosomes (C_m); as different individuals have varying C_m values that consequently result in different reflectance values. Hence, C_m is considered an unknown variable by the system. To solve this issue, melanin concentration was subsequently classified into ten groups that ranged from 1.0 to 10% at one percent intervals, for which absorption coefficients for the epidermis were calculated using Eq. (1).

$$\mu_{a,epi(\lambda)} = C_m \times \mu_{a,m(\lambda)} \quad (1)$$

where C_m is melanosome concentration and $\mu_{a,m(\lambda)}$ is the melanosome absorption coefficient. Thus, for each depth and thickness, diffuse reflectance is calculated for ten values of C_m at ten different levels, which results in 1000 simulations for each wavelength; thus equaling 3000 simulations. Different Cm curves are related later in the discussion to measured optical diffuse reflectance by means of a 'characteristic angle' that is calculated using Eq. (6), where a chromameter measures input parameters. Figure 3(a) -3(b) show variations in ratios R1 and R2 as C_m changes. During experimental trials and based on measured C_m values, one curve was selected for the derivation of R1 and R2 ratios.

Optics EXPRESS

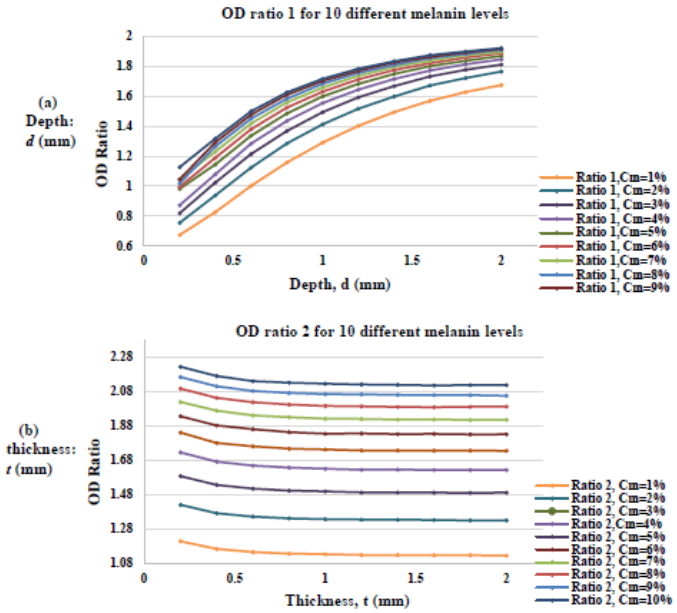

Fig. 3. (a) Evolution of ratio R1 as a function of depth for ten different C_m groups. (b) Evolution of ratio R2 as a function of thickness for ten different C_m groups; Depth and Thickness when both are set to 1mm.

As mentioned earlier, the MC model of steady-state light transport in multi-layered tissue (MCML) [27] was used to simulate light propagation in bi-layered skin tissue. Simulations were initiated with given depth and thickness values ranging from 0.2 to 2 mm (at 0.2 mm intervals) to produce 100 diffuse reflectance models per single wavelength. This is means that ten reflectance values for thickness were simulated for depth for a total of ten depths ranging from 0.2 to 2 mm (at 0.2 mm intervals); thus, 100 diffuse reflectance models were generated for each wavelength. The sequence was repeated for all three isosbestic wavelengths resulting in 300 reflectance readings for one C_m level. The entire process was then repeated for ten different C_m levels generating 3000 reflectance readings for each depth and thickness simulation. For simulation purposes, the C_b value was fixed at 0.2% for all cases, as per Jacques's proposal [30]. Regarding our earlier discussion, optical parameters for each layer of skin and for subcutaneous veins require specification prior to light propagation simulation and are also characterized as a function of wavelength (λ nm). Optical parameters for each skin layer were treated the same as the model used by Nishidate et al. [21]. Five parameters require specification for each skin and blood layer prior to simulation. These are: Scattering coefficient (μ_s); Absorption coefficient (μ_a); Anisotropy factor (g); Refractive index (n) and Thickness (t). Optical parameters for all three isosbestic wavelengths used in MCML simulations are shown in Table 1.

Table 1. Optical parameters for each skin tissue model used in MCML simulation [21].

Optical parameter	Wavelength (nm)		
	420	585	800
Absorption coefficient of melanosomes, $\mu_{a,m}$ (mm^{-1})	121.3	40.50	14.40
Absorption coefficient of blood, $\mu_{a,b}$ (mm^{-1})	230.6	18.40	0.420
Scattering coefficient of blood, $\mu_{s,b}$ (mm^{-1})	57.90	83.60	75.20
Scattering coefficient of epidermis and dermis, $\mu_{s,epi}$, $\mu_{s,der}$ (mm^{-1})	33.40	14.90	9.300
Anisotropy of blood, g_b	0.980	0.980	0.980
Anisotropy factor of epidermis and dermis, g_{epi}, g_{der}	0.740	0.790	0.850

Optics EXPRESS

Referring to Table 1, absorption coefficients for melanosomal and blood concentrations for dermis and epidermis were set at 100%. This means that at $C_m = 100 \rightarrow$ the melanosome coefficient = 121.3, and at $C_b = 100 \rightarrow$ the absorption coefficient = 230.6 at 420 nm. A similar rationalization applies to the entire Table. Epidermal and dermal thicknesses (t_e, t_d) were set to 0.06 and 4.94 mm for skin structure, respectively. The refractive index (n) was assumed to be 1.4 for all the three wavelengths, as cited in the literature [31] [32]. Nishidate et al. defined all formulae for the calculation of values for each parameter in Table 1 [21]. Our simulations therefore applied Eq. (2) to derive the absorption coefficient of the epidermis ($\mu_{a,\,epi}$):

$$\mu_{a,epi}(\lambda) = C_m \times \mu_{a,m}(\lambda) \tag{2}$$

where C_m is blood concentration, $\mu_{a,m}$ is the absorption coefficient for melanosomes.

We similarly applied Eq. (3) to derive the dermal absorption coefficient ($\mu_{a,der}$):

$$\mu_{a,der}(\lambda) = C_b \times \mu_{a,b}(\lambda) \tag{3}$$

where Cb is blood concentration and μa,b (λ) is the absorption coefficient of blood. Note that Cb was fixed at 0.2% for the calculation of the dermal absorption coefficient for all three wavelengths.

2.2 Principle of system operation

The difference in absorption between two different wavelengths at the same operative site provides data that is used to estimate both the depth and thickness of subcutaneous veins. Lesser absorption at longer wavelengths informs deeper skin penetration, whereas shorter wavelengths penetrate shallower tissues. The ratio between shallow and deeper penetrations provides data for the maximum path length of absorptive media. Hence, this convenient ratio was employed by our proposed system to estimate venous depth and thickness. The system utilizes R1 to measure depth and R2 to measure thickness, as illustrated in Fig. 4. As previously mentioned, depth and thickness measurements rely on two pillars: 1) OD ratios taken from our system, and 2) OD ratios derived from MCML simulation data. Hence, both depth and thickness are estimates derived via the system's approximation of the OD ratio in relation to the MCML simulated OD ratio. Three major alterations differentiate our proposed system from the approach offered by Nishidate et al. [21].

1. First: our system differs experimentally, as it relies on an LED lighting system compared to the filtered white light by interferential filters.
2. Second: our system *measures* C_m by chromameter and Eq. (6) rather than estimation by multi-regression analysis (MRA).
3. Third: the applicability of the proposed system was validated by 11 subjects rather than customized phantoms.

However, the method is limited to 2.0 mm determinations of thickness and depth due to the limited penetration of NIR light.

Optics EXPRESS

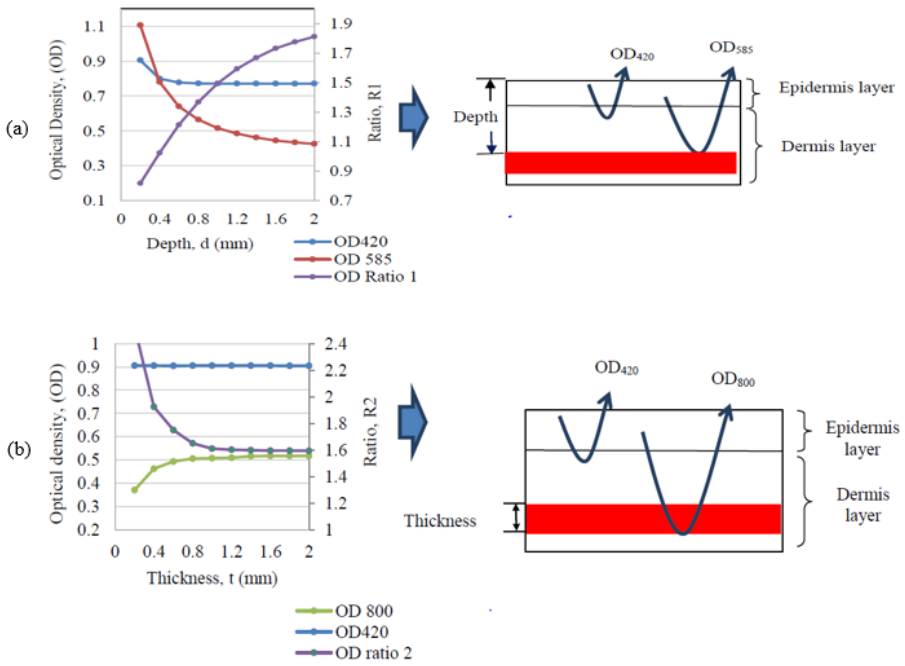

Fig. 4. (a) depth using R1; (b) thickness using R2.

We developed the proposed system in three phases:

1. Obtain input data for OD ratios (R1& R2), to include segmented vein images (mask) and 3000 diffuse reflectance models;
2. Adding a mask to OD R1 and R2 images to visualize corresponding values for OD ratios for images, respectively;
3. Estimate depth and thickness by referring system derived OD values to 3000 diffuse reflectance models according to C_m levels that were determined separately from OD measurements.

The following steps were designed to accomplish our objective of measuring venous depth and thickness based on the three cited phases. First, three images at wavelengths 420, 585 and 800 nm were captured by a two charge-couple device (CCD) camera under customized trans-illumination for a single wavelength. Second, captured images were converted into a single band for image processing. Third, single band images (I_{420}, I_{585}, and I_{800}) were normalized using Eq. (4) to obtain reflectance images R_{420}, R_{585}, and R_{800}. Fourth, these reflectance images were converted to OD images using Eq. (5). Fifth, the ratios of two OD images then obtained both OD ratios by division as follows: R1 = (OD_{420} / OD_{585}); R2 = (OD_{420} / OD_{800}). Sixth, we employed the Frangi filter to segmentally extract veins from NIR images at 800 nm [12,32]. Segmented vein images were then used as a mask for later visualization and to extract OD R1 and R2 values from R1 and R2 images, respectively. The latter values then served as input for the 3000 diffuse reflectance models to specify vein depth and thickness, as per C_m level. Equation (6) determined C_m for purposes of classifying skin tone and thus selected an appropriate curve for a specific depth and thickness. Finally, depth and thickness were obtained by referring to MCML derived R1 and R2 ratios for the diffuse reflectance model. In this step, depth and thickness were determined by R1 and R2 values obtained by the proposed optical system. All details for these processes are described in Section 3 (See: Fig. 5), which outlines all processes encompassed by the proposed system.

Optics EXPRESS

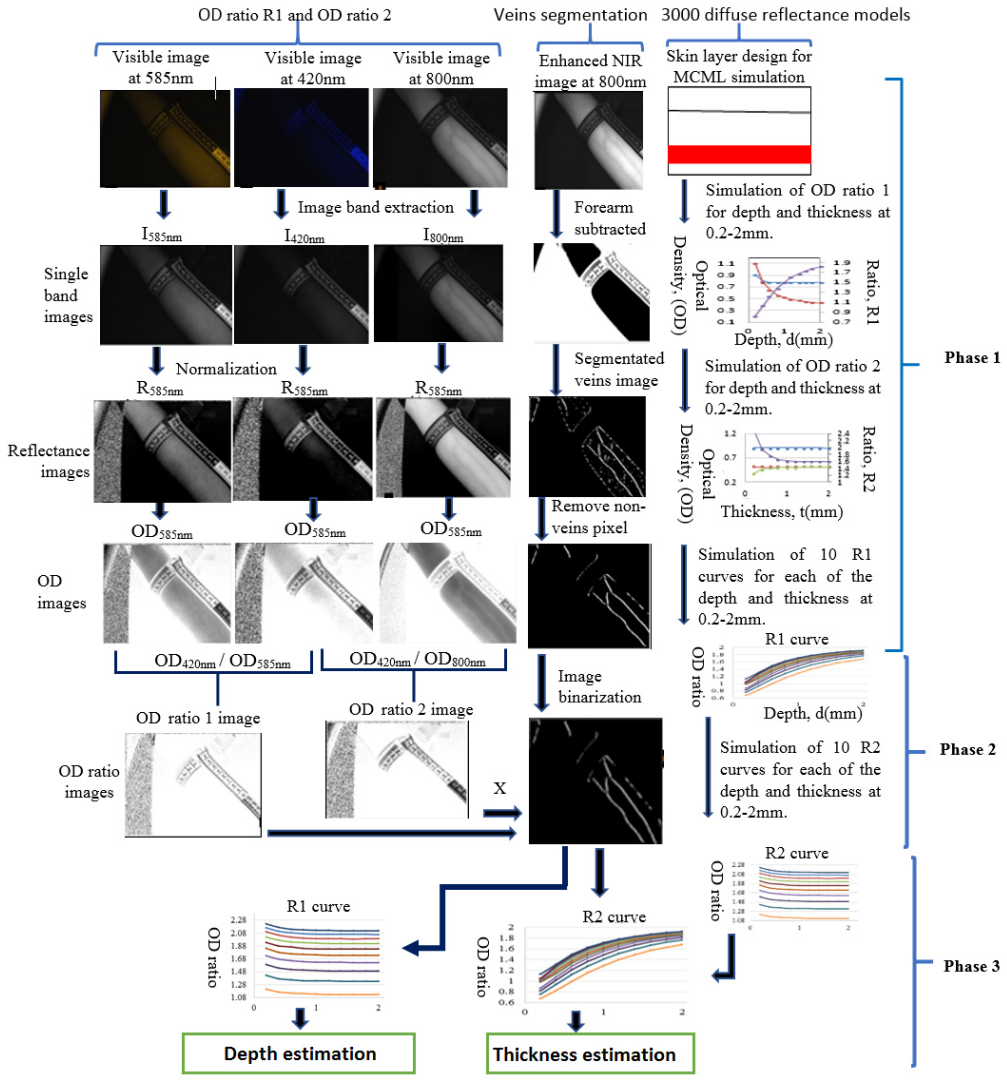

Fig. 5. Estimation processes for depth and thickness of veins using OD ratios.

3. Materials and methods

The proposed vein depth and thickness estimation system comprises hardware and software. The hardware element has three main components: Jai's 2CCD camera, an LED board with three single wavelengths, and a processing unit. The fluence rate (mW/sr) of the light at wavelength of 420nm, 585nm and 800nm are 8, 6 and 25, respectively, while the FWHM (nm) are 30, 20 and 30, respectively. We designed the software algorithm on following basis: Single band image extraction; image normalization to obtain reflectance image (Eq. (4)); conversion of the reflectance image to an optical density (OD) image (Eq. (5)); vein segmentation using the Frangi filter; processes for imaging R1 & R2; melanin concentration (C_m) (Eq. (6)); adding segmented vein images to R1 & R2 images; and venous depth and thickness value extraction by fitting OD ratio values, derived by our system, to MCML derived R1 & R2 values.

The experimental data set for research was taken from university volunteers. Selection was based on skin tone and categorized as follows: fair, light brown, dark brown and dark.

Optics EXPRESS

Luminance values (L*) were collected from participants and then clustered via fuzzy c-means (FCM) [12] into four distinct groups, and later related to a set of C_m curves to determine depth and thickness. A total of nine luminance value (L*) measurements were recorded at three separate foci (upper, center, and lower arm) and in triplicate for each subject. For the FCM algorithm, skin tones (fair, light brown, dark brown and dark) were classified based on luminance (L*) value ranges as follows: (>56.40), (49.90–56.3), (42.10–49.8) and (<42.00), respectively. Mean values for all nine readings were fed into the FCM algorithm to further objectify skin tone and validate the applicability of the proposed system for all skin tones. There were 7 fair, 1 light brown, 2 dark brown, and 2 dark toned subjects.

The 2CCD camera (JAI-AD080-CL) used for image acquisition was equipped with a visible color channel (1/3-inch Bayer Mosaic color IT CCD) plus a Near-IR channel (1/3-inch monochrome IR IT CCD). This camera has a resolution of 1024 (h) x 768 (v) active pixels per channel [cell size: 4.65 (H) x 4.65 (V) μm)] and is able to simultaneously capture co-registered images in both visible and Near-IR spectra via the same optical path. One should note that all the images at different wavelengths are capture separately and the images of Visible and NIR are co-registered. The bit depth for the CCD of NIR and visible images are 8 bits and 24 bits (8 bits per channel) respectively. The camera has a maximum programmable exposure time of 33 μs and master gain of −3 dB to + 12 dB. To obtain uniform illumination of any scene of interest, the LED board was custom fit with 145 LEDs for three wavelengths placed in four concentric circles with radii of 6, 7, 9, and 11 cm, respectively. Each concentric circle held three LED types (three wavelengths), all arranged in alternating sequence (See Fig. 5). Inner (1) to the outer ring (4) held 60, 45, 30, and 15 LEDs, respectively. Butter paper was applied as a diffuser to better ensure homogenous light distribution. LEDs were controlled by a customized interface for each wavelength and triggered per capture to obtain single wavelength images. A 64-bit processing unit with PCI slots and a 2.5 GHz processor, compatible with a frame grabber card (Dalsa X64-CL (DUAL 66 MHz with 32 MB), were used to acquire images at 640 x 480 pixels.

Figure 6 depicts the setup of the proposed measuring system. While acquiring images, the camera exposure time was adjusted so that diffuse reflectance images from the skin surface obtained maximum intensity for all three wavelengths without reaching sensor saturation. The light of the three wavelengths (420nm, 585nm and 800nm), gain was set at 792 for all the three wavelengths and the exposure time are set as follows: (10μs), (32μs), (27μs), respectively. The gain and exposure time were first set for the white calibration plate and the same settings were used for the black calibration plate and for forearm imaging during acquisition. The camera was placed 280 mm from the bench top surface to optimize focus with respect to a Region of Interest (ROI) and was surrounded by illuminant LEDs placed in a circular pattern to project homogenous lighting onto the forearm. The assembly was tilted at ~80 degrees and focused on the ROI. The forearm was positioned diagonally to the ROI to maximize exposure within the field of view.

Optics EXPRESS

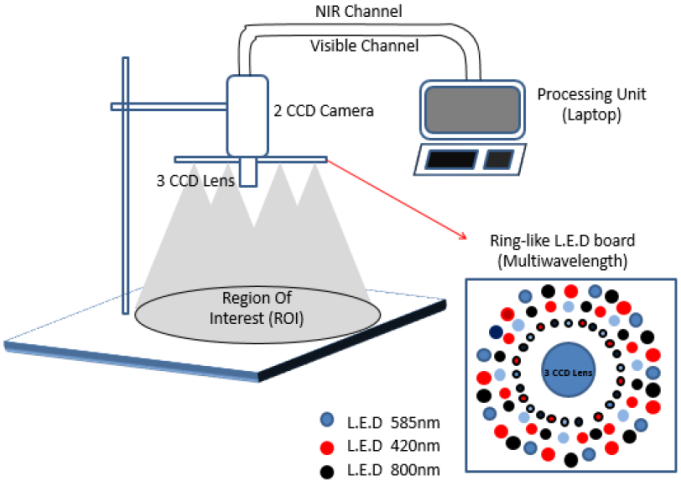

Fig. 6. Vein depth and thickness measuring system.

Artifacts were reduced by following few steps with respect to the system, environment and the subjects. Including a diffuser to distribute the incident light homogenously and minimized the system 'noise'. Controlling the illumination setting of the environment reduced the environmental perturbations. The motion artifacts were minimized by fixating the position of the forearm under the centroid of the light beam and the subject was instructed to minimize voluntary movement during the acquisition procedure. In case of movements, seen by comparing the images acquired at different wavelengths, the data were not taken into account. The system was left running for few hours and the grey level of the acquired images were found to be constant over time, showing the stable lighting illumination as well as a non-noticeable acquisition noise.

3.1 Algorithm design for the estimation of venous depth and thickness

This sub-section describes the algorithm we specifically designed to accommodate the various methodologies and working principles of the proposed system. The first step in the processes acquires separate images for each isosbestic wavelength for hemoglobin (I_{420}, I_{585}, I_{800}). Note that CCD sensors are switchable and were changed when taking images for different spectra. Flexible tape was attached to the forearm to serve as a reference guide for later comparisons with Ultrasound data results for validation purposes. Subjects were asked to position the forearm for the ROI and not to move during image acquisition. LEDs were switched on after subjects were ready, as per instruction, and only one LED type at a time acquired a single wavelength image.

For the second step, single-band image extraction was performed for images at visible wavelengths. NIR images are consisted with three bands (RGB). Nonetheless, only the one band that maximized intensity for a respective wavelength was needed for image processing. According to spectra responses from our color CCD sensor, peak responses to 420 nm lay only on the blue band [33], whereas for 585 nm, it was between green and red bands [33]; thus, only the blue band was used for imaging at 420 nm, whereas mean data from red and green band results were used for imaging at 585 nm. For NIR images, peak monochrome sensor responses were obtained at 800 nm and it has only one band of image, therefore, NIR images did not require further processing.

During the third step, captured images in a single band were normalized to obtain reflectance images using Eq. (4) [34]. In normalization, known reflectance values for black and white calibration plates were set at 0.95 and 0.10, respectively. Exposure time and gain were adjusted so that diffuse reflectance from each skin layer achieved maximum readings

Optics EXPRESS

without saturating the sensor. Normalized images for all three wavelengths were obtained separately, as they have independently calibrated values.

$$R(x,y,\lambda)=\frac{[I(x,y,\lambda)-I_2(x,y,\lambda)]\times R_1-[I(x,y,\lambda)-I_1(x,y,\lambda)]\times R_2}{I_1(x,y,\lambda)-I_2(x,y,\lambda)} \quad (4)$$

where $I\ (x, y, \lambda)$ is the forearm image; $I_1\ (x, y, \lambda)$ is the image acquired for the white calibration plate; $I_2\ (x, y, \lambda)$ is the image acquired for the black calibration plate; R_1 is the reflectance index for the white calibration plate; and R_2 is the reflectance index for the black calibration plate. Next (fourth step), normalized images were converted to OD images using Eq. (5).

$$OD(\lambda)=-Log(R) \quad (5)$$

OD images for all three wavelengths were then used to generate images of R1 and R2. In this process, the forearm's position for all images should be same for all three wavelengths. This is because the ratio of two images should reference the same position for purposes of comparison. Prior to the inference of depth and thickness by OD ratio determination, the melanosome concentration (C_m) was independently calculated using Eq. (6), where L* and b* values were measured by chronometer (Konica Minolta). The C_m value was then calculated and categorized as per Eq. (6) [34]. L* and b* values had been measured during experimental processing prior to image acquisition. A 'characteristic angle', as obtained during this process, was then determined and used to select the appropriate C_m group for use in the determination of depth and thickness.

$$\alpha=\tan^{-1}\left(\frac{L^*-50}{b^*}\right) \quad (6)$$

where α is the characteristic angle; L^* is lightness; and b^* is the yellow/blue coordinate.

We determined the C_m group as per the method of G. Zonios et al. [34], by plotting melanin content as measured on UVB-irradiated skin sites against the 'characteristic angle' (α) (See: Fig. 7). As shown in the graph, results indicated that the Y-intercept was 100 and the X-intercept was ~50.55. We then derived the linear equation, based on these points, to characterize melanin content as a function of the 'characteristic angle'. Hence, melanin content, as determined by the derived linear equation, and the 'characteristic angle', were independently calculated. This parameter correlated well with the appearance of skin color [35]. An experiment was performed to validate the correlation between melanin content on UVB-irradiated skin sites and measurement via Eq. (6). Experimental results empirically demonstrated that the correlation between both parameters was good ($r = 0.96$, $p < 0.001$); thus confirming Eq. (6) application for melanin content.

Optics EXPRESS

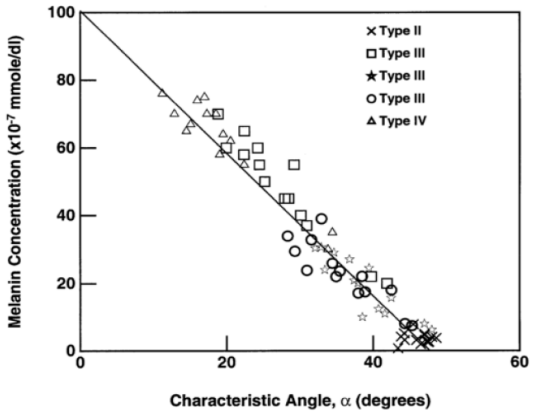

Fig. 7. Melanin content results for UVB-irradiated skin sites taken from five subjects (Skin Type II–IV) vs. corresponding values of the 'characteristic angle' (α).Reproduced from [35].

This was followed by vein segmentation using the Frangi filter, as applied to NIR images at wavelength 800 nm, to extract veins from the raw image. Segmented vein imaging is used to specify the location of veins and extract the OD ratio values (R1 and R2). Finally, the obtained OD ratio is referred to the 3000 diffuse reflectance models to produce depth and thickness, accordingly. Figure 8 shows an example of the depth and thickness measurement process for the proposed system.

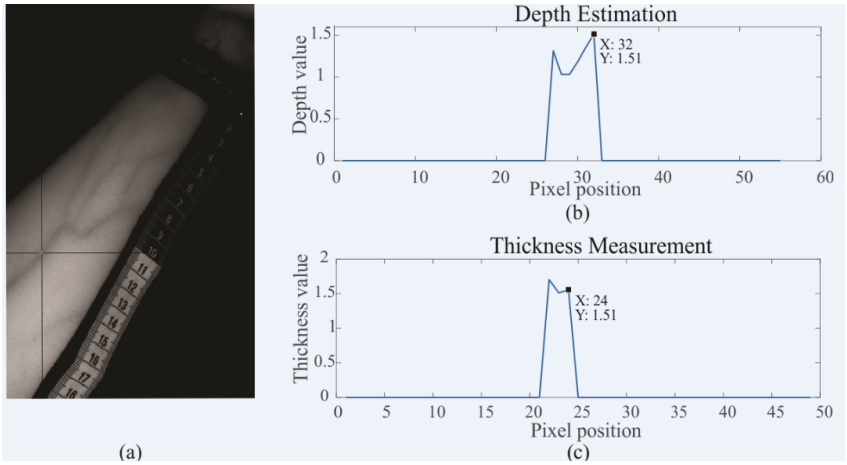

Fig. 8. (a) Selecting a point from fused images to extract values of: (b) depth and (c) thickness using the proposed imaging system.

As a summary to above mentioned processes of proposed system, Fig. 9 showed the process flow of the proposed imaging system to estimate the depth and thickness as per mentioned above.

Optics EXPRESS

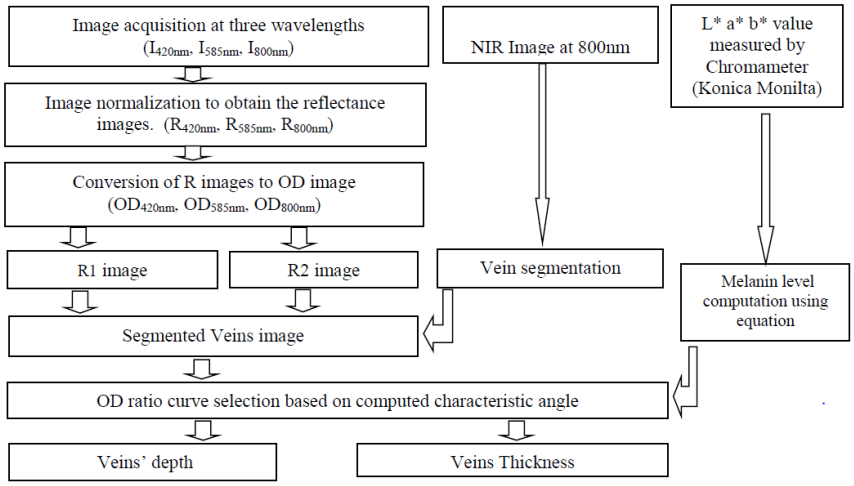

Fig. 9. Summarizes process flows for the proposed system.

After venous depth and thickness were determined, results were compared with in vivo ultrasound measurements. We used Toshiba's Xario US unit with a transducer of 12 Mega Hertz to identify a vein at a specified point. These measurements then served as ground truth to validate results obtained by the proposed optical method. A power Doppler was employed to properly visualize tiny subcutaneous veins. Images were magnified 1.5 X. A linear transducer was used to probe a specified point for reference as indicated by the flexible tape seen in Fig. 8. The transducer was longitudinally oriented and target measurements were correlated with optic measurement points. Figure 10 shows ultrasound measurement results obtained by the linear transducer.

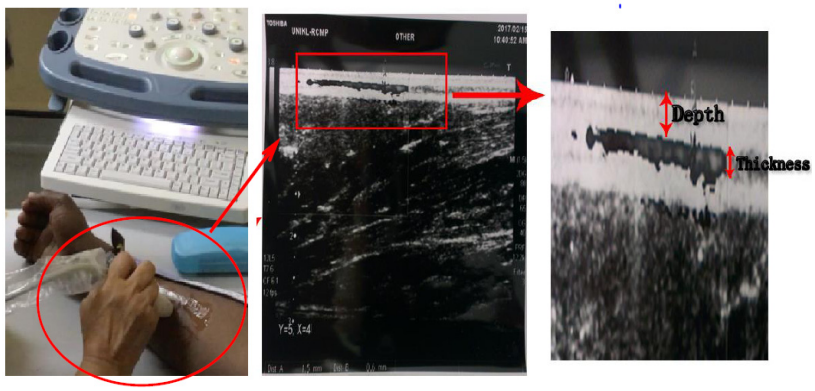

Fig. 10. Depth and thickness measurement using an ultrasound linear transducer.

4. Results and discussion

Experimental results were obtained from 66 optic points for 11 subjects (six probe points per subject: 6 fair, 2 light brown, 1 dark brown, 2 dark). Ultrasound measurements for vein depth and thickness were performed at the same sites. Readings for both data sets were independently recorded. Figure 11 shows correlations between these data sets for all 66 points and 11 subjects.

Optics EXPRESS

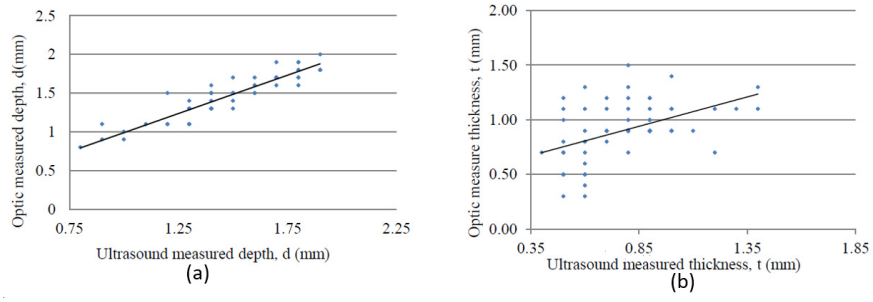

Fig. 11. Correlations between ultrasound and optical assays for **(a)** depth and **(b)** thickness.

Comparative results for the statistical relations between both data sets were in good agreement for depth: R^2 = 0.843 and regression analysis indicated a CI of 95%, which confirmed the applicability of the system for the measurement subcutaneous vein depth. However, we a obtained a weak correlation for thickness measurements, where R^2 = 0.221. This is possibly due to errors that can be attributed to ultrasound measurement. Thickness readings were simply not uniform along the line of the transducer probe and indicated a need for further investigation. Figure 12(b) shows variation in thickness measurements obtained by the transducer probe corresponding with five points used for the optical assay. Referring to Fig. 12(a), we see that ultrasound depth measurements (from skin surface to the upper surface of the vein) were consistent when compared to ultrasound thickness measurements (Fig. 12(b)). However, measurements from a vein's anterior wall to its posterior wall fluctuated along the probe's length. From observation, we can assume that ultrasound readings might not be the actual points that would otherwise more correctly correspond with optic measurements. On the other hand, the excess pressure by the transducer could give a false thickness due to the fact that the veins have collapsible walls.

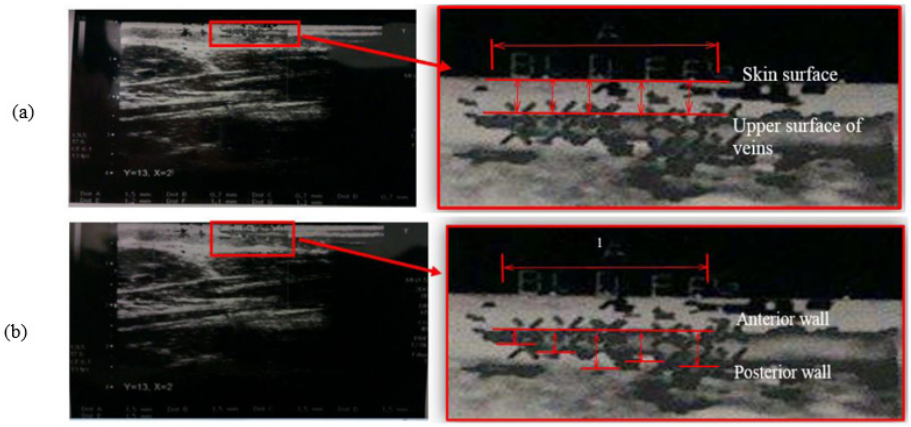

Fig. 12. Ultrasound measurements: (a) depth, (b) thickness.

To further investigate the cited discrepancies in thickness measurements, multiple ultrasound measurements were repeated at optic measurement sites. Six ultrasound measurements taken from two different subjects were repeated in an attempt to match optical measurements. A total of 66 ultrasound measurements were thus performed for six optical measurements on subject 1 and five optical measurements on subject 2. Here, thickness results obtained by the proposed optical system served as references for ultrasound measurements to validate 'tolerance' for thickness measurements. Figure 13(a)-13(b) show these experimental results for subject 1 and subject 2.

Optics EXPRESS

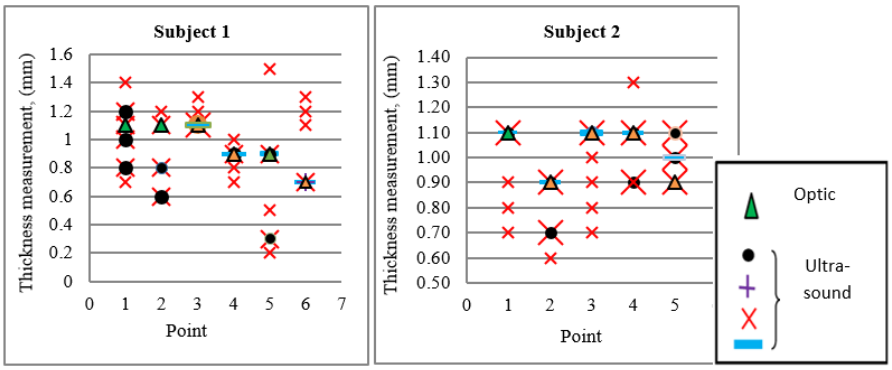

Fig. 13. Tolerance of thickness measurements for the two subjects.

Once again, we noted that ultrasound measurements fluctuated compare to optical measurements, ranging from 0.2 to 1.5 mm. Therefore, it is likely that these results indicate that ultrasonic measurements are inappropriate for the evaluation of our system with regard to vein thickness. Nonetheless, results did demonstrate that values obtained by our proposed system were aligned within the range of ultrasound results; thus, indicating the system works; however, at the same time our system prevents us from interpreting results in terms of accuracy. On the other hand, the excess pressure by the transducer could give a false thickness due to the fact that the veins have collapsible walls. In order to validate the tolerance of thickness measurement based on optic measurement, the six ultrasound readings of each optic measurement points are averaged. This average value is then minus with the optic measurement to obtain the discrepancy. Table 2 below shows the discrepancy of each optic measurement point for subject 1 and subject 2. 'Discrepancy' is defined as the absolute difference between the mean of ultrasound to the optic measurement.

Table 2. The discrepancy of thickness measurement between ultrasound and optical measurement.

	Subject 1			Subject 2		
Point	Optic (mm)	Mean of ultrasound (mm)	Discrepancy (mm)	Optic (mm)	Mean of ultrasound (mm)	Discrepancy (mm)
1	1.1	1.022	0.078	1.1	0.95	0.15
2	1.1	0.850	0.250	0.9	0.78	0.12
3	1.1	1.150	0.050	1.1	0.96	0.14
4	0.9	0.867	0.033	1.1	1.07	0.03
5	0.9	0.656	0.244	0.9	1.02	0.12
6	0.7	0.950	0.250	1.1	0.956	0.112
Average			0.151			0.15

According to the result in Table 2, we found that the total discrepancy of ultrasound measurement to the optic measurement for subject 1 and subject 2 are 0.151mm and 0.15mm respectively. Besides that, Body mass index (BMI) is one of the limitation in our optic measurement system. To validate the influence of BMI index to the measurement of depth and thickness, eight subjects were selected and classified into three group: (a) Group 1: BMI = 20 – 25, (b) Group 2: BMI = 25 – 30 and (c) Group 3: BMI = 30 – 35. The number of subjects in group 1, group 2, and group 3 are 2, 4, and 2 respectively (Fig. 14).

Optics EXPRESS

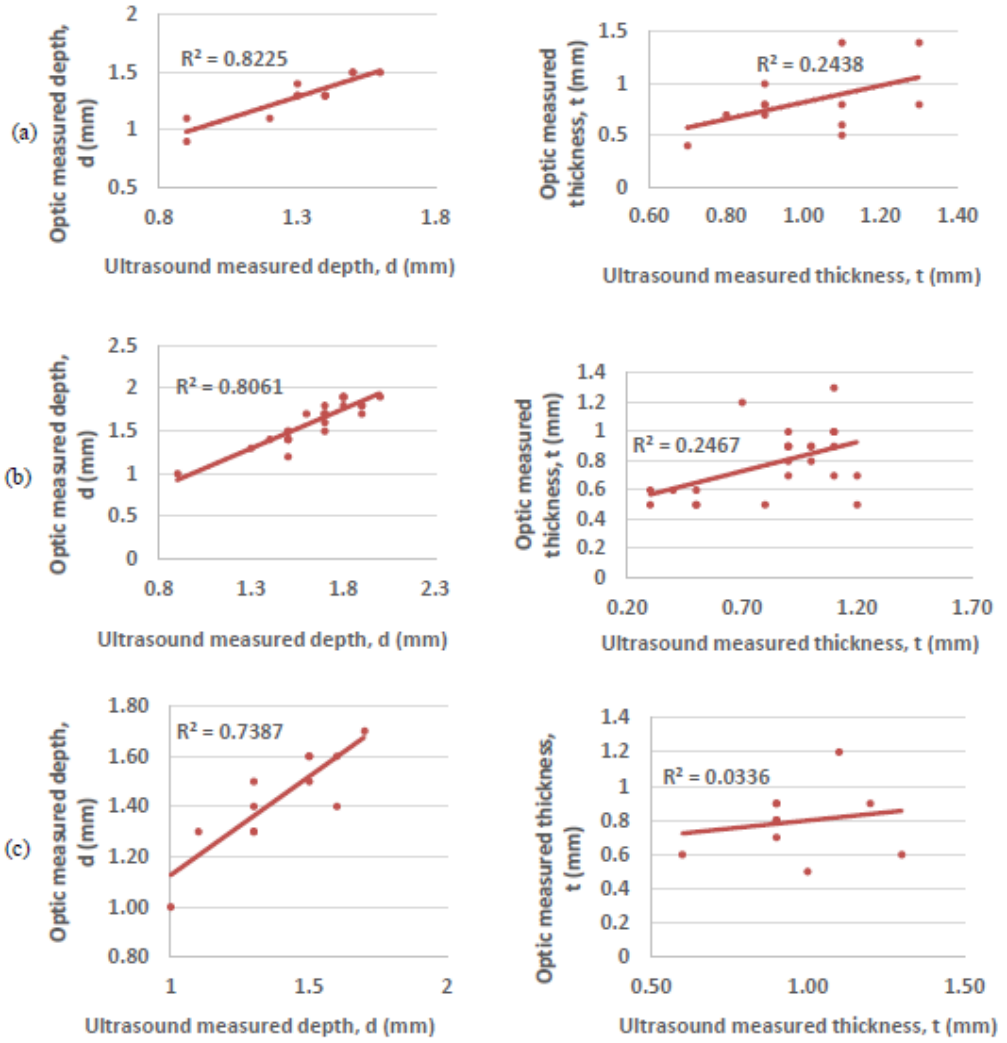

Fig. 14. Correlation measurements between ultrasound and optic based on vary BMI index: (a) Group 1: BMI = 20 – 25, (b) Group 2: BMI = 25 – 30 and (c) Group 3: BMI = 30 – 35.

Table 3 summarized the correlation measurement of depth and thickness between ultrasound and optic based on the BMI index.

Table 3. R^2 value for depth and thickness between ultrasound and optic based on BMI index.

Group	Depth	Thickness
1, BMI = 20-25	0.8225	0.2438
2,BMI = 26-30	0.8061	0.2467
3, BMI = 31-35	0.7387	0.0336

From the results as shown in Table 3, we found that the R^2 value for the measurement of depth and thickness are inversely proportional to the BMI index. The R^2 values decrease when the BMI index increases. This trend indicates that the BMI index should be taken into account in the model for high BMI index. On the other hand, to help validate the applicability and effectiveness of the proposed system to measure subcutaneous vein depth and thickness for patients with different skin tones; results were further broken down in accord with one

Optics EXPRESS

distinct skin tone. As mentioned previously, 11 subjects were selected of which, 6 were fair, 2 were light brown, 1 was dark brown and 2 were dark skin types. The correlations for overall results in terms of R^2 values were 0.822 and 0.203 for depth and thickness, respectively. For light brown, dark brown and dark skin tones, R^2 values for depth and thickness were 0.822 & 0.244; 0.827 & 0.069; and 0.868 & 0.741, respectively. Figure 15 shows the linear regression fit for all skin tones.

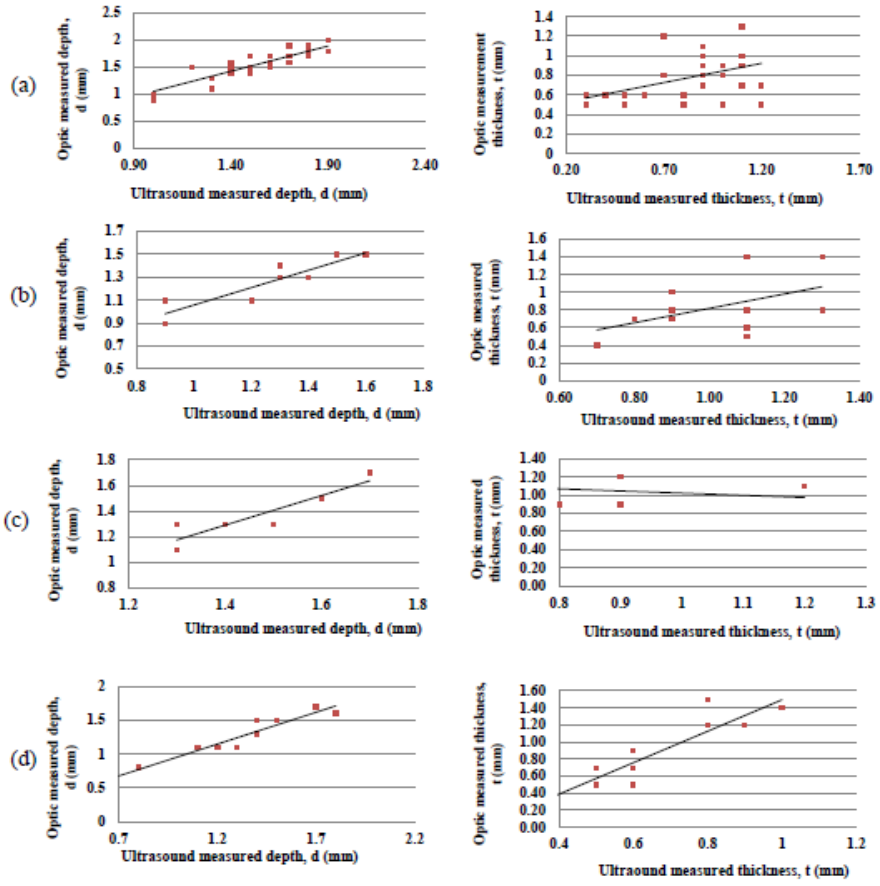

Fig. 15. Correlation measurements between ultrasound and optic measurements for one distinct tone: (a) fair, (b) light brown, (c) dark brown, (d) dark.

To verify the system effectiveness for all type of skin tones, Table 4 summarizes R^2 results and tolerance values for each distinct tone measurement.

Table 4. Values for R^2 and tolerance of depth and thickness for all skin type measurements.

	Depth		Thickness	
Skin tone	R^2	Tolerance (mm)	R^2	Tolerance (mm)
All four skin tone (11 Subjects)	0.843	0.090	0.278	0.210
Fair (6 Subjects)	0.822	0.080	0.251	0.175
Light Brown (2 Subjects)	0.822	0.070	0.248	0.267
Dark brown (1 Subjects)	0.827	0.100	0.120	0.200
Dark (2 Subjects)	0.870	0.133	0.347	0.741

Optics EXPRESS

Tolerance values for the proposed system's measurement of depth and thickness for all skin types (66 points) were 0.09 mm and 0.21 mm, respectively. These results indicated that depth and thickness measurements varied by 0.09 and 0.21 mm, respectively. The cause of variation in thickness measurements was discussed in the previous section. The study by Nishidate et al. [21] showed error rates of 30 and 19%, respectively, for in-vivo depth and thickness measurements. Compared to our system's results, their R^2 values were 0.843 and 0.221 for depth and thickness measurements, respectively. Our system demonstrated improved accuracy for both measurements in terms of statistical analysis.

As for additional measurements of depth and thickness for single tones, experimental results demonstrated a tolerance range from 0.07 to 0.133 mm, meaning that our system offers a maximum depth discrepancy of 0.133 mm for dark skin types and a minimum discrepancy of 0.07mm for light brown skin. In terms of general practice, a maximum tolerance of 0.133 mm for depth is insignificant for IV procedures. Hence, the proposed optic system is indeed feasible for the measurement of subcutaneous vein depth. Nonetheless, for thickness measurement, it is not possible to quantitatively conclude validity as explained above (See: Fig. 13) because of the high degree of variability in obtained ultrasound readings. Further investigation will be done to validate this discrepancy. NB: According to the state of the art, the standard C_b is 0.2% and no other values were reported. Therefore, variation in reflectance could not be related in this study to any discrepancy in thickness.

5. Conclusion and future work

This paper proposed a new measurement system that infers both the depth and thickness of subcutaneous veins with a view to improve the success rate of venous access in IV procedures. We presented a detailed discussion of the estimation processes of the proposed system. We also discussed the system's effectiveness and accuracy with comparisons of in vivo results with in vivo ultrasonic measurement. The project's next phase aims to enhance the sensitivity for measuring Cm with a different approach to the method proposed by Nishidate et al. [21], which is to determine Cm via multiple regression analysis (MRA) using an obtained OD value. Moreover, we plan to reconstruct 3-D subcutaneous vein images using data of depth as obtained by our proposed system. Such 3-D vein imaging can possibly serve to guide an autonomous venipuncture robot [25]. Moreover, 3-D ultrasound can guide a surgical robot's [36] orientation to drive the needle during the puncture of a pre-designated vein. For depth measurement, reports from an autonomous venipuncture robot program indicated a depth resolution range of 0.1 to 0.2 mm, while a 3-D ultrasound guided surgical robot reported an rms error of 1.34 mm. Compared with a tolerance of 0.09 mm obtained by our proposed system, this encourages efforts to improve efficiency and accuracy for both devices.

Funding

Ministry of Higher Education (MOHE) Malaysia under the Fundamental Research Grant Scheme (FRGS), cost centre no. 0153AB-K02.

Acknowledgments

This work was undertaken at Universiti Teknologi PETRONAS and Universiti Kuala Lumpur (Unikl) in collaboration with the University Bourgogne Franche-Comte.